International Journal of Biological Macromolecules 254 (2024) 127689

Contents lists available at ScienceDirect

International Journal of Biological Macromolecules

journal homepage: www.elsevier.com/locate/ijbiomac

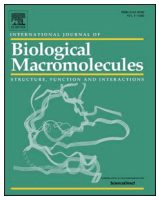

Fabrication of double layer nanoparticle infused starch-based thermoplastic food packaging system for meat preservation

Chandra Mohan Chandrasekar *, Luca Nespoli, Tommaso Bellesia, Masoud Ghaani, Stefano Farris, Diego Romano

Department of Food Environmental and Nutritional Sciences, University of Milan, Italy

ARTICLE INFO

Keywords:
Thermoplastic films
Starch
Nanoparticles
Interaction
Diffusion
Preservation

ABSTRACT

The current work aims to produce nanoparticle-infused starch-based bioactive thermoplastic packaging films. The FeO and ZnO nanoparticles were examined to be potential active ingredients for the production of nanoparticle-infused bioactive thermoplastic packaging films. The bio-thermoplastic films infused with FeO and ZnO nanoparticles showed high oxygen scavenging and antimicrobial activity, respectively. Consecutively, both films were combined to form a double-layer Nano-Biothermoplastic packaging system for food preservation. The distribution and diffusion of nanoparticles in starch-based films were examined to be influenced by the amorphous character of starch and the swelling index of the film, respectively. The amorphous property of starch molecules showed a masking effect on the crystalline characteristics of nanoparticles in Nano-Biothermoplastic films. The diffusion of nanoparticles from the Nano-Biothermoplastic packaging system was found to influence the microbial, chemical, and color characteristics of mutton and chicken meat stored at 4 °C.

1. Introduction

The accumulation of synthetic plastics derived from petrochemicals is a serious problem that affects the environment. Many research works are being done to produce natural polymers to replace synthetic polymers [1–4]. Therefore, polymers such as starch and cellulose which are abundant in nature, have been the subject of rigorous investigations [4–6]. The starch molecules have reforming capabilities when subjected to gelatinization and retrogradation, which is why they are referred to as bio-thermoplastics. The bio-thermoplastics are eco-plastics that consist of naturally formed polymers or biologically derived polymers. These bio-thermoplastics can be broken down into simple monomers by microbes present in soil and atmosphere. Thus, they are eco-friendly and can reduce environmental pollution [7].

The starch molecules (consisting of crystalline amylose and amorphous amylopectin) can be a potential source for the production of bio-thermoplastic film. The cellulose molecules with their high crystalline nature can be a potential reinforcing agent for improving the barrier properties of the bio-thermoplastic films. The integrity of cellulose-reinforced starch-based bio-thermoplastic films is mainly dependent on the interaction between the amorphous amylopectin in starch with crystalline cellulose [1,7]. The starch-based bio-thermoplastic films don't have innate preservative capabilities to act as an active packaging system since they are susceptible to microbial contamination. Therefore, active ingredients can be infused into bio-thermoplastic films to improve their antioxidant and antimicrobial properties. In recent years, several researchers have worked on the infusion of various active ingredients into bio-thermoplastic films [8–10]. Among the investigated active ingredients, nanoparticles are fascinating active ingredients with a broad application-oriented property. The ZnO nanoparticles are interesting in their food packaging applications because of their significant antimicrobial properties, non-toxicity, UV protection, high thermal stability and surface-to-volume ratio [11]. The FeO nanoparticles with high oxygen scavenging properties can be an effective active ingredient in food packaging applications [12]. Detailed studies on the diffusion of nanoparticles into food products have profound importance, for the production of nanoparticle-infused bio-thermoplastic films.

This work is the continuation of the previous works, 1) 'Extraction

Abbreviations: TVC, total viable count; PM, *Pseudomonads*; LAB, *Lactobacilli*; EB, *Enterobacteriaceae*; MWNF, meat without Nano-Biothermoplastic film; NC, negative control (meat wrapped in biothermoplastic films without nanoparticles); PC, positive control (meat wrapped with biothermoplastic films containing commercial BHT); NP, meat samples wrapped with Nano-Biothermoplastic films.

* Corresponding author.
E-mail address: chandra.chandrasekar@unimi.it (C.M. Chandrasekar).

https://doi.org/10.1016/j.ijbiomac.2023.127689
Received 22 April 2023; Received in revised form 11 June 2023; Accepted 24 October 2023
Available online 1 November 2023

and Characterization of polysaccharides from tamarind seeds, rice mill residue, okra waste and sugarcane bagasse for its Bio-thermoplastic properties' [2] and 2) 'Effect of film constituents and different processing conditions on the properties of starch-based thermoplastic films' [7]. In the first work polysaccharides from different agro-industrial wastes were extracted and characterized for their properties, then in the second work the thermoplastic film-forming capabilities were examined for the extracted polysaccharides. The reported insights from those initial works: 1) The starch molecules extracted from tamarind seed wastes contain a high amount of amylose as well as xyloglucan (linear polysaccharides) with good film forming capability. 2) Mucilage polysaccharide extracted from okra head portion waste was examined to have repeating units of α - (1,2)-rhamnose and α - (1–4) -galacturonic acid residues with disaccharide side chains. We observed that okra mucilage has very good hydrogen bonding capabilities and can serve as a good natural plasticizing additive in starch/cellulose-based thermoplastic films. Thus, we used the okra mucilage extracted in the initial work as a natural plasticizer in this work. 3) Cellulose extracted from sugarcane bagasse can be a good reinforcing agent for starch based thermoplastic films. The clove extract has good antioxidant properties with high polyphenols [1] and it can serve as a potential reaction solution for green synthesis of nanoparticles [13]. The main aim of the present work is, to develop nanoparticle-infused starch-based bioactive thermoplastic packaging films. Moreover, this work also aims to study the interaction, diffusivity, bioactivity, and preservation potential of Nano-Biothermoplastic packaging films.

2. Materials and methods

2.1. Overview of the initial works

The polysaccharides from tamarind seed, okra head, and sugarcane bagasse agro-industrial wastes were extracted and characterized for their polymer properties [2]. The derived polysaccharides were optimized for the fabrication of starch-based thermoplastic packaging films [7].

2.2. Overview of the works reported in this manuscript

This work can be separated into four parts. First part: Production and characterization of FeO and ZnO nanoparticles. Second part: Development and characterization of Nanoparticle infused bio-thermoplastic packaging films. Third part: Examining the diffusion kinetics of nanoparticles from Nano-Biothermoplastic packaging film into the chicken and mutton meat. Fourth part: Examining the effect of the Nano-Biothermoplastic packaging system on microbial, chemical, and color characteristics of chicken and mutton meat.

2.3. Raw materials

The okra mucilage polysaccharide, tamarind seed starch, and sugarcane bagasse cellulose from our previous study [2] were used for the fabrication of Nano-Biothermoplastic films. The aqueous extract of clove was extracted by dissolving 10 g of clove powder in 100 mL of sterile deionized water, subjected to shaking of 500 ×*g* at room temperature for 15 h. The resultant extract was filtered, freeze-dried, and stored at −20 °C until further use. The chicken meat (70.1 g/100 g moisture, 22.9 g/100 g protein, 2.1 g/100 g fat content) and mutton meat (60.3 g/100 g moisture, 17.3 g/100 g protein, 16.5 g/100 g of fat content) were procured from local slaughtering house (Chennai, Tamilnadu, India). The meat samples were collected in insulated polystyrene boxes (kept at 4 °C) and transferred within 30 min to the laboratory. The analytical chemicals and solvents used in this study were procured from Merck Millipore (Merck Specialities Pvt. Ltd.). Purity: EMPARTA^{ACS} grade for analysis. The media components and microbial culture media were procured from Hi-media laboratories.

2.4. Synthesis of FeO and ZnO nanoparticles

The ZnO and FeO nanoparticles were produced by reducing the salts of zinc acetate and (Ferric and ferrous sulphate mixture in the ratio of 0.8). Different concentrations (1, 5, 10, 15, and 20 mM) of zinc acetate and (ferric and ferrous sulphate mixture) salt solutions were mixed with 20 μg/mL aqueous extract of clove. The mixture was subjected to a constant stirring of 500 ×*g* at 35 °C for 1 h, with nitrogen sparging at the rate of 10 cm^3/min. The resultant solution was dried in a hot air oven at 90 °C and calcinated/annealed at 200 °C using a muffle furnace. The resultant particles were kept in glass ampoules for further use.

2.5. Characterization of FeO and ZnO nanoparticles

The produced ZnO and FeO nanoparticles were analyzed for their UV absorbance [14,15], Particle size [2,16], Morphology [7,17], Zeta potential [18], Functional groups [19], Antioxidant and Antimicrobial properties [1,9]. The detailed procedures for the above-mentioned analyses of Nanoparticles are given as Supplementary Data from Sections 2.2.1 to 2.2.7.

2.6. Production of Nano-Biothermoplastic packaging films

1.50 g/100 mL okra mucilage, 4 g/100 mL tamarind seed starch, and 1.5 g/100 mL cellulose were dissolved in deionized water to prepare bio-thermoplastic films. The resultant matrix solution was gelatinized at 90 °C for 5 min. After gelatinization, nanoparticles at MIC concentration levels of (ZnO - 40 μg/mL) or (FeO - 60 μg/mL) were added into the matrix of the edible film. The film-forming solution was poured on a petri dish (diameter 15 cm) and dried at 60 °C for 3 - 4 h. A double-layer packaging system was produced by adding ZnO to the matrix and dried to form a stable film. Then the film matrix solution containing FeO was poured over the dried ZnO film and dried to form a double-layered packaging film.

2.7. Characterization of Nano-Biothermoplastic packaging films

The film samples were conditioned for 10–15 days at constant 50 % humidity, to avoid errors due to the absorption of moisture by the films. The Nano-biothermoplastic films were characterized for their Morphology [7,17], Mechanical properties [7], Oxygen Transfer Rate (OTR) [20], Water Vapor Permeability [21], Swelling Index [22] and Diffusion kinetics of nanoparticles in the food samples (meat system) [23]. The detailed procedures for the above-mentioned analyses of Nano-Biothermoplastic packaging films are given as Supplementary Data from Sections 2.4.1 to 2.4.6.

2.7.1. Diffusion kinetics analysis of nanoparticles in the solid meat system

2.7.1.1. Thickness optimization of meat samples. The optimization of meat thickness was done as per the method mentioned in our earlier work [23,24]. Meat samples with a postmortem age of 30 min were stored at 4 °C. They were then cut into 1 × 1 cm portions with different thicknesses ranging from 0.2 to 3 cm (0.2, 0.5, 1, 1.5, 2, 2.5, 3 cm). Before packing the meat samples, the initial load of microorganisms in the meat was determined as per the method mentioned below. Nanoparticle-infused films (~0.45 mm thick) were placed on one side of sliced meat (perpendicular to muscle fiber of longer axis) and aseptically sealed in polyethylene bags. Bags were stored at 4 °C. After storing for 24 h, the film was detached from the meat surface and the side of the meat which is not in interaction with the film was placed over the surface of nutrient agar plates for a few minutes. Both film and meat samples were discarded and the agar plates were incubated for 24 h at 37 °C. Microbial load in meat (after 24 h) was taken as an index for the optimization of meat thickness. The maintenance or reduction of the

initial load of microbes was measured as a breakpoint for the selecting thickness of meat or the least inhibition of microbial load.

2.7.1.2. Kinetic of nanoparticles in the meat system. The pieces of Nanoparticle infused film (1.5 × 1.5 cm^2) were placed over meat slices (postmortem age of 30 min and pH of 6.82 ± 0.16) at optimized thickness. Meat samples were sampled every 2nd day for 34 days. The nanoparticle-containing meat samples were put in storage at temperature conditions of 4 °C and 10 °C. The diffusivity of nanoparticles was studied over the storage period. The extent of nanoparticles released into the meat during the period was calculated by examining the amount left back in the film (that covers the meat). During each sampling process (to estimate the number of nanoparticles left back in the film), a piece of film was taken out from the sample (meat) and put into a glass tube containing 2 mL of PBS solution. The solution containing the film was kept for 6 h under shaking. After this incubation period, the concentration of nanoparticles (FeO and ZnO) in PBS solution was measured using atomic absorption spectroscopic analysis. The below-mentioned formula was used to compute the fractional release of nanoparticles (AT_R) into the meat samples from the films.

$$AT_R = 1 - \left(\frac{AT_{t=i}}{AT_{t=0}}\right) \tag{1}$$

where the amount of nanoparticles at the time (i) present in the film is given as $AT_{t=i}$, the amount of nanoparticles present at the time (0) in the film is given as $AT_{t=0}$. The fractional release of nanoparticles from the films into the meat samples was examined and plotted with time (t).

A mathematical model was used to predict the release of nanoparticles from the film matrix. The mechanism of release was presumed to be by diffusion. Based on the structural characteristics of the matrix polymer and its swelling behavior, the pattern of release is expected to differ. It was also assumed that (1) primarily, there was a homogenous distribution of nanoparticles concentration in a thin sheet of the film; (2) diffusion of nanoparticles was considered to be perpendicular to the film surface and unidirectional; (3) the film is in full contact with meat surface. Since tamarind seed starch is hydrophilic, water diffusion in a hydrophilic system was considered for the model. Two phenomena occur in this system: stochastic phenomenon (associated with Brownian motion), where the flow penetrating substance is driven by concentration difference and relaxation phenomenon is driven by the system to attain equilibrium [23]. The model system used in our work is a combination of polymer relaxation and stochastic phenomena. The diffusion coefficients were determined using a relationship derived from Fick's law for a plane sheet developed by Crank [25].

For the diffusion of nanoparticles from films into the meat (at a fixed temperature), mathematical parameters were computed using the equation [22]:

$$M(t) = M_{eq}\cdot\left\{X_F\cdot\left\{1 - \frac{8}{\pi^2}\cdot\sum_{n=0}^{n=\infty}\frac{1}{(2n+1)^2}\cdot exp\left[-D\cdot(2n+1)^2\cdot\pi^2\cdot\frac{t}{l^2}\right]\right\} + (1 - X_F)\cdot\left[1 - exp\left(-\frac{t}{\tau}\right)\right]\right\} \tag{2}$$

where M(t) - the amount of nanoparticles diffused into meat at time t; M_{eq} - the amount of nanoparticles diffused into meat at equilibrium condition (under stochastic phenomena); X_F - deviation of nanoparticle diffusion from Fickian behavior. Note: deviation of X_F ranges from 0 to 1; The above-mentioned equation provides a solution for Fick's second law if $X_F = 1$ and denotes anomalous diffusion at $X_F = 0$; D - diffusivity coefficient; l - meat thickness; t - the time of sampling; τ - relaxation time of polymer. The fractional release (predicted) of nanoparticles from the film surface into the meat ($M(t)/M_{eq}$) was examined and plotted with time (t).

The resistance offered to the flow of nanoparticles by the solid medium can be expressed from the equation [25].

$$R = \frac{L}{D} \tag{3}$$

where, R – Resistance; L – length or thickness of the solid matrix; D – active compound Diffusivity.

The Iron, and Zinc concentrations were examined regularly through atomic absorption spectroscopy, to evaluate the diffusion of nanoparticles [26,27]. The Hitachi 170–50 (Japan) atomic absorption spectrometer (flame type) with cathode lamps (hollow) was used for the analysis. The parameters of the instrument were set as per the recommendations of the manufacturer. A Zn and Fe cathode lamp (hollow) operating at 213.9 nm and 248.3 nm was used as a source of radiation for the analysis of zinc and iron present in packaging films. The cathode lamp was fixed at 15 mA. The composition of flame was: air (at pressure 1.5 kg/cm^2), and propane-butane (at pressure 0.1 kg/cm^2). The film (1 g) was heated at 512 °C using a muffle furnace, to produce ash. Before analysis, ash was diluted with 2 % (w/v) HNO_3. The zinc and Iron stock solutions (standard at 1000 mg/L), were diluted with concentrated nitric acid (analytical grade) and deionized water to make working standards of various concentrations. The 2 % (w/v) HNO_3 solution was used as a calibration blank. Working standards for iron and zinc were (1, 5, and 10 mg/L) and (0.5,1 and 2 mg/L) respectively.

2.8. Effect of nano-biothemoplastic packaging on the shelf-life of chicken and mutton meat

2.8.1. Meat sample preparation

Meat samples (postmortem age of 30 min and stored at 4 °C) were sliced to optimized thickness. The samples were then wrapped with nanoparticle-fused bio-thermoplastic films, then the samples were stored at 4 °C to conduct shelf-life analysis. The meat samples covered in bio-thermoplastic films (without nanoparticles) were taken as the negative control. The meat samples wrapped in 0.02 g/100 mL of BHT (Butylated hydroxytoluene) incorporated films were taken as a positive control. The microbial parameters were examined once in 5 days until the TVC of the sample crosses 7 Log CFU/g (acceptable limit) [28]. The protein oxidation, color, and TBARS of meat were also studied at the same time interval until the acceptable shelf life of the sample.

2.8.2. Microbial examination of meat samples

The microbial quality of the sample enfolded with nanoparticle-fused film and control film was analyzed on each sampling day. The 10 g of meat samples were aseptically homogenized (Model PT-MR-2100, Kinematica AG, Switzerland) with 90 mL (0.1 %) sterile peptone water and the same was used to make serial dilutions. Microbial parameters such as *Pseudomonads*, *Enterobacteriaceae*, *Lactobacillus*, and Total Viable Counts (TVC) were computed.

The 100 μL of serially diluted and homogenized meat sample was plated on plate count agar for TVC analysis. Plates were incubated for 48 h at 37 °C. The colony counter was used to count the microbial colonies. The *Pseudomonads* counts were enumerated using pseudomonas agar with Cetrimide – Fucidin – Cephaloridine after incubating the plates at 25 °C for 48 h. *Lactobacillus* MRS agar was used to determine *Lactobacillus* count after incubating the plates at 37 °C for 72 h. The violet red bile glucose agar was used to compute *Enterobacteriaceae*

count after incubating the plates for 48 h at 30 °C. Microbial parameters were expressed as Log CFU/g.

2.8.3. Protein oxidation and TBARS analysis of meat

2-Thiobarbituric acid analysis (TBARS) or secondary lipid oxidation of meat samples was examined as per the method mentioned by Chandra Mohan et al. [24]. The level of TBARS was recorded as milligrams of malondialdehyde per kilogram of the sample (mg MDA kg^{-1} of meat) [29].

The total carbonyl content or the Protein oxidation (PO) of meat was quantified as per the procedure mentioned by Chandra Mohan et al. [23,24]. Using Bovine Serum Albumin (BSA) as standard, protein concentration in the sample was calculated by measuring the absorbance at 280 nm. The carbonyl content was given as nmol of carbonyl per mg of protein.

2.8.4. Analysis of meat color

The color parameters of meat samples were examined with Hunter Lab Ultra Scan VIS color spectrophotometer (Hunter Associates Laboratory Inc., Reston, VA, USA). The instrument was calibrated against black and white reference tiles. The CIE color values were obtained from illuminant A (light source). The port size (diameter) and area view were 1.02 cm and 0.64 cm^2, respectively. The angle of observation was set at 10°. The obtained color values were used to calculate the color of meat (ΔE) using the equation given by Chandra Mohan et al. [23]. Where, $_0$ - 0th-day value, L* - lightness value, a* - redness value and b* - yellowness value.

$$\Delta E = \sqrt{\left(L^* - L_0^*\right)^2 + \left(a^* - a_0^*\right)^2 + \left(b^* - b_0^*\right)^2} \quad (4)$$

2.9. Statistical analysis

All the studies were carried out in triplicates to find standard deviation and mean values. Duncan's multiple ranges and one-way Analysis of variance tests were done for mean values to assess the significant differences between the values. IBM SPSS software (version 22) and Microsoft Excel Data Analysis Centre (2010) were used for statistical data analysis.

3. Results and discussions

3.1. Synthesis and characterization of ZnO and FeO nanoparticles

Fig. 1A depicts the UV absorption bands of the ZnO and FeO nanoparticles. Generally, nanoparticles strongly absorb blue transition light between UV and visible spectra. This absorption is called the blue shift phenomenon that takes place because of the quantum confinement effect in nanoparticles [14]. The peak absorption of the blue shift phenomenon was noted at 395 and 364 nm for FeO and ZnO nanoparticles, respectively. The absorption of FeO Nano suspension made from 1 mM salt solution was observed to be considerably ($P < 0.05$) higher than other investigated concentrations. The absorption of ZnO Nano suspension made from 10 mM salt concentration solution was observed to be considerably ($P < 0.05$) higher than other investigated concentrations. This significant difference may be dependent on the concentration and quality of nanoparticles in the suspension [15,30]. The plain salt solution of the respective nanoparticles was found to have insignificant ($P > 0.05$) absorption in the blue shift phenomenon range. This could be due to a lack of nanoparticles in the salt solution.

The particle size, nano conversion rate, and zeta potential of the produced nanoparticles were tabulated in Table 1. The least average size of ZnO nanoparticles was observed to be 61.09 ± 0.22 nm for the particles produced from 10 mM salt concentration, with a maximum nano conversion percentage of 95.45 ± 0.25 %. The least average size of FeO nanoparticles was observed to be 79.63 ± 0.24 nm for the particles produced from 1 mM salt concentration, with a maximum nano conversion percentage of 98.34 ± 0.19 %. This considerable difference ($P < 0.05$) in size and conversion percentage of nanoparticles from other investigated salt concentrations could be because of the optimized interaction of polyphenolic components present in aqueous clove extract with metallic salts [31]. The surface charge of a nanoparticle in a colloidal solution can be determined from zeta potential measurement. The nanoparticles have a surface charge that draws a thin layer of ions to the surface of the nanoparticle. This double ion layer migrates through the solution along with the nanoparticles. The electrical potential at the periphery of the double layer is known as the zeta potential of the particle and has a value that usually ranges from +100 to −100 mV [32].

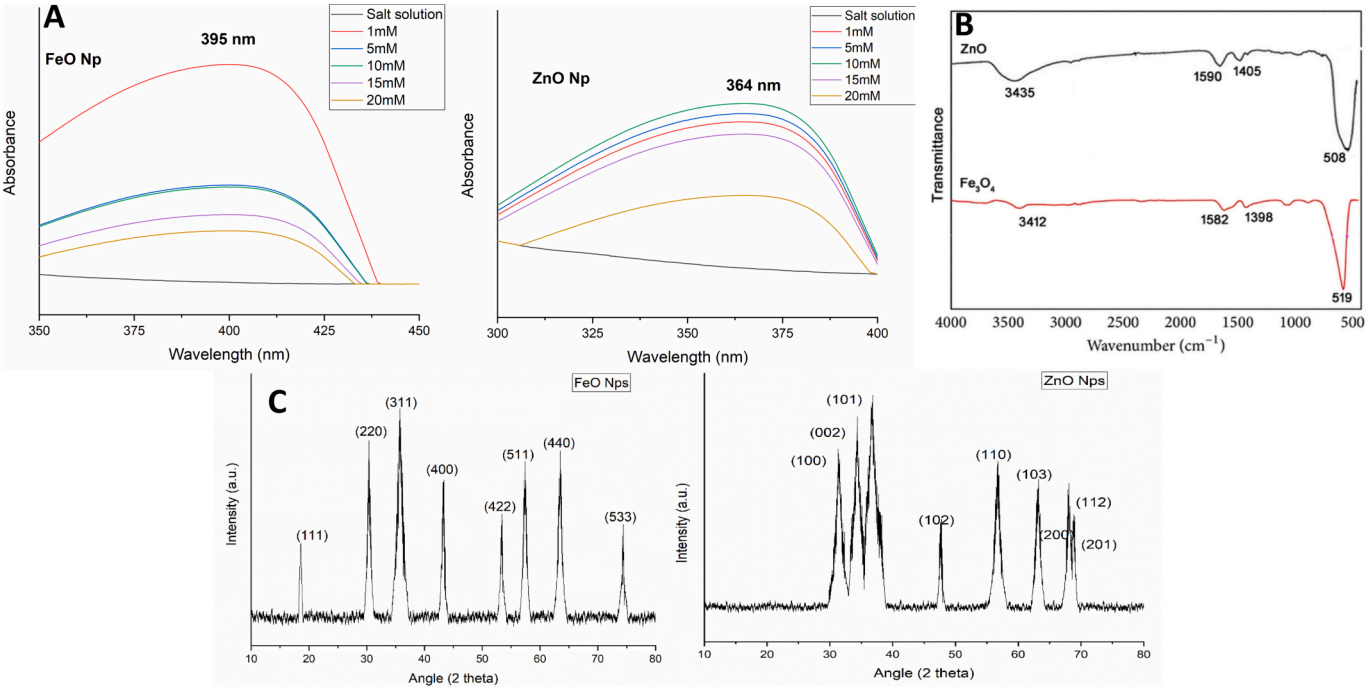

Fig. 1. A – UV Absorbance Spectra of Nanoparticles; B – FTIR Spectra of Nanoparticles; C – X-Ray Diffraction Spectra of Nanoparticles.

Table 1
Particle size, conversion rate, and zeta potential of iron and zinc-based nanoparticles.

Concentration	ZnO Np			FeO Np		
	Average particle size	Nano conversion	Zeta potential	Average Particle size	Nano conversion	Zeta potential
Unit	nm	%	mV	nm	%	mV
1 mM	63.68 ± 0.38	95.35 ± 0.23	26.8 ± 0.11	79.63 ± 0.24	98.34 ± 0.19	−24.1 ± 0.15
5 mM	61.83 ± 0.13	93.22 ± 0.41	25.6 ± 0.13	96.37 ± 0.18	87.27 ± 0.24	−22.3 ± 0.11
10 mM	61.09 ± 0.22	95.45 ± 0.25	28.9 ± 0.17	106.54 ± 0.37	85.19 ± 0.17	−23.1 ± 0.15
15 mM	70.38 ± 0.18	87.28 ± 0.27	27.5 ± 0.14	106.98 ± 0.21	79.62 ± 0.22	−21.8 ± 0.17
20 mM	78.67 ± 0.26	85.19 ± 0.21	25.8 ± 0.12	109.37 ± 0.32	78.41 ± 0.27	−23.6 ± 0.16

The nanoparticles with zeta potential values of more than +25 mV or less than −25 mV usually have a high level of stability [33]. The nanoparticles with zeta potential that falls in between this range will not be stable, they will agglomerate and will lose their characteristic size. The nanoparticles with zeta potential farther away from this range will be more stable [32]. The zeta potentials of ZnO and FeO nanoparticles were examined to be around (25.6–28.9 mV) and (−21.8 to −24.1 mV), respectively. These zeta potential results indicate the moderately stable nature of produced ZnO and FeO nanoparticles.

Fig. 1B illustrates the FTIR spectra of ZnO and FeO nanoparticles. The intense band at 508 and 519 cm^{-1} confirms the stretching vibrations of Zn—O [34] and Fe—O [35], respectively. The other minor bands were noticed in ~1590, ~1400, and ~3400 cm^{-1} corresponding to C—H stretching, C—C stretching and O—H stretching, respectively. These minor peaks could be due to trace amounts of carbon and hydrogen-containing compounds from clove extract, even after complete calcination of nanoparticles at 200 °C. Similar observations were reported by Khalil et al. [36] during the synthesis of FeO nanoparticles with *Sageretia thea* (Osbeck) aqueous extract.

The X-ray diffraction spectra of FeO and ZnO Nanoparticles are illustrated in Fig. 1C. The XRD diffraction spectra of ZnO nanoparticles revealed the octahedral and tetrahedral structural pattern of pure magnetite FeO nanoparticles, with crystallographic reflections of (111), (311), (220), (422), (400), (440), (533) and (511) [37]. It should be noted that magnetites and maghemites are isostructural patterns, which means that the XRD technique cannot clearly distinguish them. Especially in a nanophase state their characteristic reflection is wide and occurs at almost the same 2θ position. The diffraction spectra of ZnO nanoparticles revealed pure wurtzite structural pattern, with crystallographic reflections of (100), (101), (002), (110), (102), (200), (103), (201) and (112) [34,38]. The characteristic peaks were examined to be broad; this may correspond to the nanometer scale of the particles [38].

The scanning electron microscopic images of FeO and ZnO nanoparticles are depicted in Fig. 2. The FeO nanoparticles were examined to be in the shape of a sphere with particle sizes ranging from ~90.89 to 64 nm. The nanospheres of ZnO nanoparticles were observed to be forming agglomerates, this phenomenon may be ascribed to the moderate stability of FeO nanoparticles evaluated in zeta potential analysis. The ZnO nanoparticles were examined to be in the shape of sharp flakes with particle sizes ranging from ~94 to 50 nm. The ZnO nanoflakes were examined to be forming ball-like structures (Fig. S1). A similar occurrence was also reported by [39] during the chemical production of ZnO nanoparticles.

Table 2 tabulates the antimicrobial and antioxidant properties of FeO and ZnO nanoparticles. The ZnO nanoparticles produced in 10 mM concentration trails with an average particle size of 61.09 ± 0.22 nm and Zeta potential of 28.9 ± 0.17 mV were used for the analysis as well as for the production of ZnO infused Nano-Biothermoplastic Films. This ZnO nanoparticles trail concentration was chosen due to its significantly high nano conversion rate (>95 %). The FeO nanoparticles produced in 1 mM concentration trails with an average particle size of 79.63 ± 0.24 nm and Zeta potential of −24.1 ± 0.15 mV were used for analysis as well as for the production of FeO-infused Nano-Biothermoplastic films. This FeO nanoparticles trail concentration was chosen due to its significant nano conversion rate as well as the size of nanoparticles which were below 100 nm. The ZnO nanoparticles were found to be having high antimicrobial properties with low minimum inhibition concentrations against investigated food spoilage microbes. Castro-Mayorga et al. [39] investigated the effect of ZnO nanoparticles on the development of L. *monocytogenes* and *S. enterica* and reported that the ZnO nanoparticles

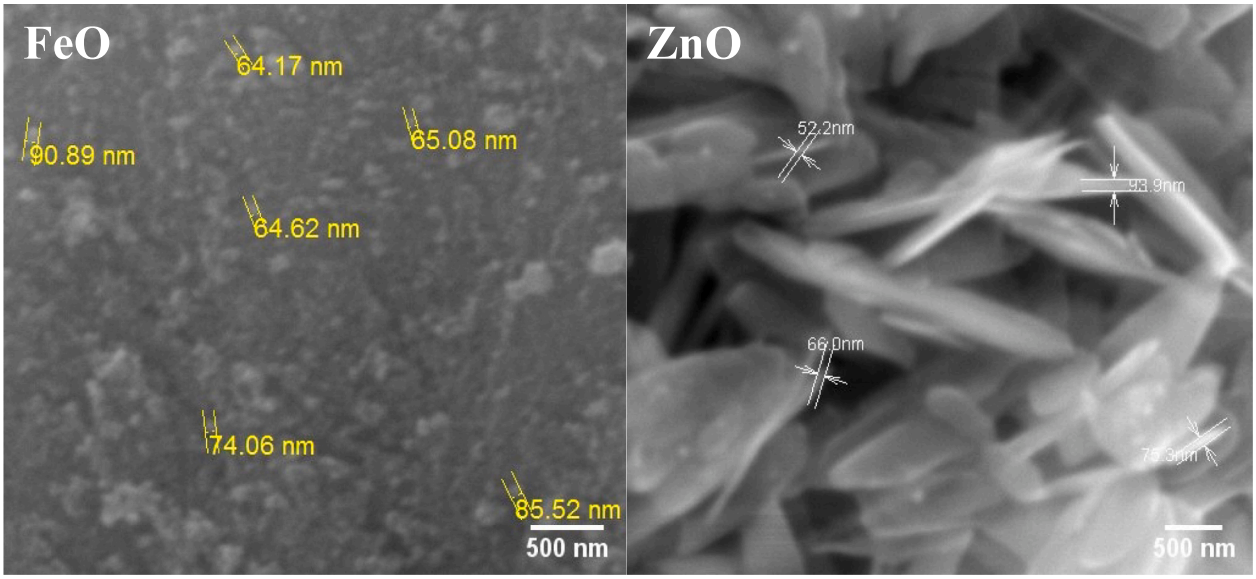

Fig. 2. Scanning electron micrographs of Nanoparticles.

Table 2
Antioxidant and antimicrobial potential of ZnO and FeO nanoparticles.

Parameter	ZnO Np	FeO Np	ZnO Np	FeO
Antimicrobial analysis	Zone of inhibition (mm)		Minimum inhibition concentration (μg/mL)	
Escherichia coli	22.53 ± 0.6	15.68 ± 0.3	30	60
Salmonella sp.	28.36 ± 0.4	19.75 ± 0.4	20	30
Shigella flexneri	30.18 ± 0.2	20.22 ± 0.2	30	30
Vibrio parahaemolyticus	25.74 ± 0.5	16.38 ± 0.8	40	60
Vibrio cholerae	27.22 ± 0.7	17.25 ± 0.5	40	50
Pseudomonas aeruginosa	28.68 ± 0.1	16.87 ± 0.3	30	50
Lactobacillus delbrueckii	35.74 ± 0.7	20.24 ± 0.2	20	40
Brochothrix sp.	30.87 ± 0.5	19.11 ± 0.6	30	50
Antioxidant analysis	DPPH radical scavenging assay		ABTS radical scavenging assay	
μ mol TE/g	6.53 ± 0.62	7.87 ± 0.57	3.28 ± 0.41	4.64 ± 0.38

are effective in the reduction of microbial growth by >6 Log CFU. Talebian et al. [40] reported that the antimicrobial property of the nanoparticles could be related to the effectiveness of larger particle surface area which may enhance the surface reactivity. Recently Krishnamoorthy et al. [41] studied the antimicrobial mechanism of ZnO nanoparticles and revealed that there are two mechanisms involved in the antimicrobial nature of ZnO particles. The first mechanism is that ZnO elevates the level of reactive oxygen species (ROS) and malondialdehyde in the bacterial cells as membrane disruptors. The second mechanism is that ZnO nanoparticles diminish the permeable membrane, denature the intracellular proteins, and cause DNA damage with membrane leakage. Based on their findings, the action of ZnO nanoparticles has been reported to have broad-spectrum antibacterial action. Similarly, FeO nanoparticles were reported to elevate reactive oxygen species (ROS) to facilitate antimicrobial activity [42,43]. But it has not yet been observed to cause broad-spectrum antimicrobial action, compared to ZnO nanoparticles. The antioxidant capacity of FeO nanoparticles was observed to be considerably ($P < 0.05$) higher than the ZnO nanoparticles. This may be ascribed to the oxygen absorption capacity of FeO nanoparticles [12].

3.2. Production and characterization of Nano-Biothermoplastic films

The produced nanoparticles (ZnO - 40 μg/mL; FeO - 60 μg/mL) were infused into the tamarind seed starch-based bio-thermoplastic packaging films to examine its mechanical properties, oxygen transfer rate (OTR), water vapor permeability, internal and external morphology. Table 3 tabulates the mechanical strength, permeability, and swelling index of nanoparticle-infused starch-based thermoplastic films. Generally, addition of nanoparticles in to film matrix solutions improves the mechanical properties of the film. But in our study, the nanoparticle infusion into the starch films was observed not to influence the mechanical properties and swelling index of the films. This may be attributed to the low concentration of nanoparticle infusion in to the film matrix, which is not significant enough to show evident change in mechanical properties. But a considerable difference ($P < 0.05$) in oxygen permeability was observed for iron nanoparticle-infused starch films, in comparison with TS films. This phenomenon may be ascribed to the high oxygen-scavenging activity of FeO nanoparticles [12].

The scanning electron surface micrographs of ZnO and FeO nanoparticle-infused starch films are depicted in Fig. 3A. The nanoparticle-infused films were observed to have a smooth surface. This may be ascribed to the homogeneous mixing of nanoparticles with a film solution matrix [11]. The nanoparticles were observed to be embedded in the matrix of the bio-thermoplastic films. This could be because of the immobilization of nanoparticles by the polysaccharide matrix. The nanoparticle size was observed to be increased inside the starch-based bio-thermoplastic films. This phenomenon may be ascribed to the coating/covering effect of nanoparticles by amorphous amylopectin molecules present in starch.

The internal morphology of the nanoparticle-infused bio-thermoplastic films was illustrated through cross-sectional SEM analysis and XRD spectral analysis of films. The scanning electron cross-sectional micrographs of TS and nanoparticle-infused films are depicted in Fig. 3B. The XRD spectra of nanoparticle-infused films are depicted in Fig. 3C. The nanoparticles were observed to be small dots embedded throughout the cross-section of the film. Babaei-Ghazvini et al. [14] reported that the film preparation method, type of polymer, concentration of film matrix, and nanoparticles influence the distribution of nanoparticles inside the film matrix. Therefore, the even distribution of the nanoparticles observed in the starch bio-thermoplastic films may be attributed to the immobilization capacity of amylopectin molecules present in starch. Ni et al. [11] studied the XRD arrangement of ZnO-infused starch films and reported that the films did not exhibit the typical peaks of ZnO nanoparticles. But in our study, the typical nanoparticle peaks were observed in both ZnO and FeO-infused bio-thermoplastic films. This could be due to the even distribution of nanoparticles noted in the cross-section micrograph of films. The intensity of characteristic crystalline peaks in both nanoparticle-infused films was observed to be affected by the film matrix. This significant decrease ($P < 0.05$) in crystalline peaks of XRD confirmed the masking effect of amorphous starch against the crystalline property of nanoparticles infused into the film.

Fig. 4, depicts the FTIR spectra of nanoparticle-infused bio-thermoplastic films. The characteristic IR spectral peaks at ~3000–3500 cm^{-1} (O—H stretches), ~2900 cm^{-1} (C—H stretch), ~1300–1600 cm^{-1} (C—C stretches/bends), and ~ 1000 cm^{-1} (C—O—C glycosidic linkages between glucose monomers) were noted in starch-based bio-thermoplastic

Table 3
Mechanical strength and oxygen transfer rate of nanoparticles infused tamarind seed starch films.

Parameters	Unit	ZnO film	FeO film	TS films
Average Thickness	mm	0.44 ± 0.12	0.46 ± 0.09	0.49 ± 0.15
Tensile strength	MPa	10.19 ± 1.58	10.21 ± 1.25	10.22 ± 1.72
Elongation	%	62.18 ± 1.51	62.22 ± 1.67	62.18 ± 2.71
Young's modulus	MPa	16.38 ± 1.09	16.40 ± 1.14	16.43 ± 1.23
Oxygen transfer rate	$cm^3 \mu m m^{-2} d^{-1}$ kPa^{-1}	13.89 ± 2.39	8.06 ± 1.17	14.11 ± 4.71
Water vapor permeability	$g\ s^{-1} m^{-1} Pa^{-1}$	0.59 ± 0.05	0.62 ± 0.07	0.61 ± 0.09
Swelling Index	%	61.87 ± 2.47	62.18 ± 2.88	62.41 ± 3.14

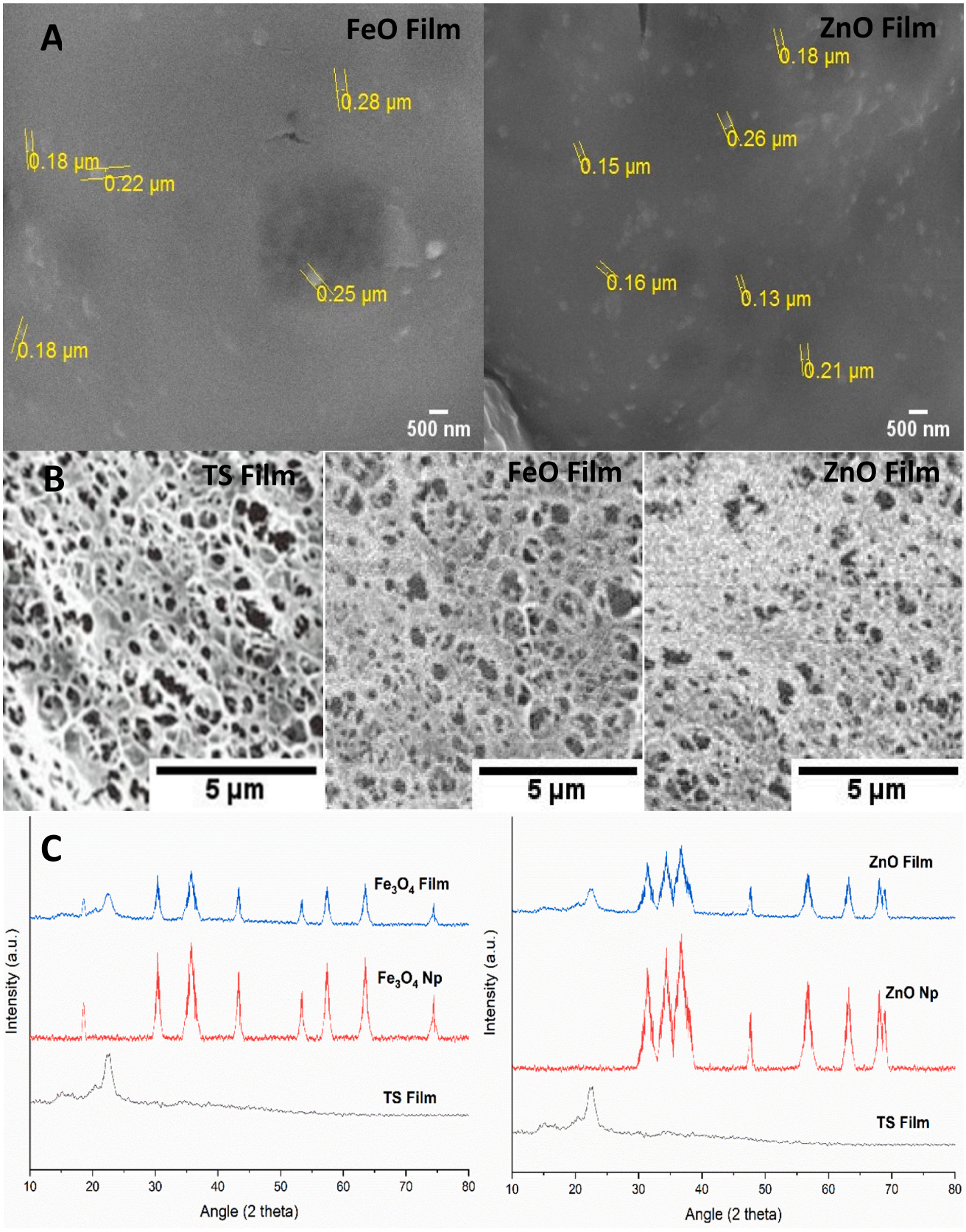

Fig. 3. A - Scanning electron micrographs of Nanoparticles infused Biothermoplastic films (Surface morphology); B - Scanning electron cross-sectional micrographs of Nanoparticles infused Biothermoplastic films (Internal morphology); C - XRD spectra of Nanoparticles infused Biothermoplastic films.

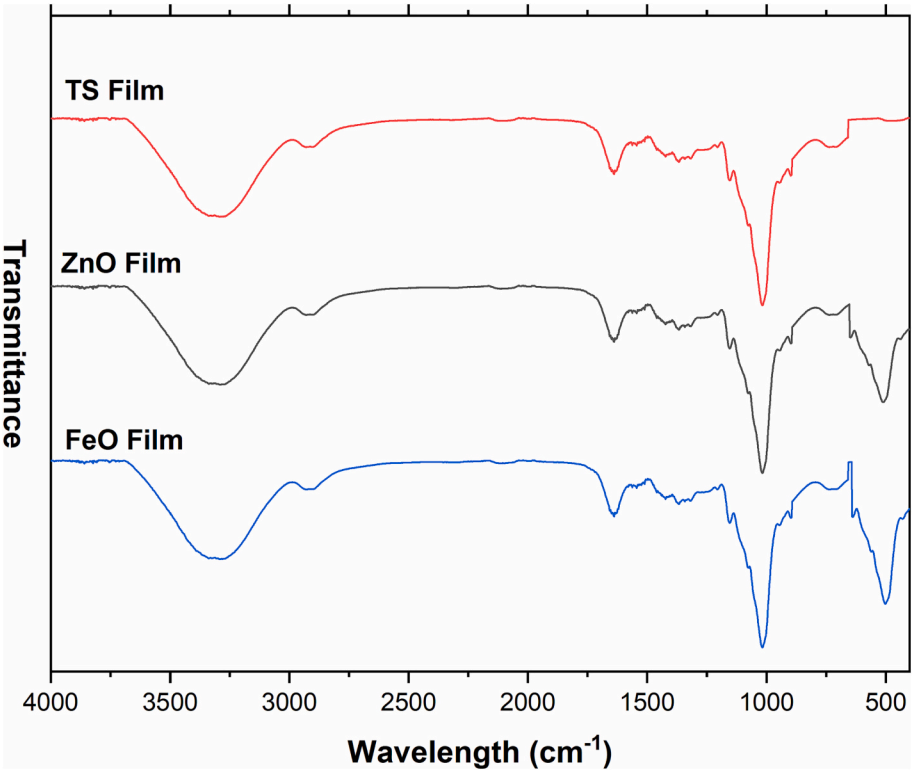

Fig. 4. FTIR spectra of nanoparticle infused biothermoplastic films.

film [2,9]. The characteristic peak of nanoparticles (Fe—O and Zn—O stretch) was noted at ~500 cm^{-1} [36,39], in addition to the other characteristic peaks of bio-thermoplastic film. There was no additional peak or shifts that were observed in both the nanoparticle-infused films which may be ascribed to a lack of strong chemical interaction between infused nanoparticles and film matrix. Therefore, the interaction between nanoparticles and the film matrix of bio-thermoplastic films could be because of weak hydrogen bonding, as was already observed in the nanoparticle immobilization effect of starch through SEM analysis.

From the overall characterization of Nano-Biothermoplastic packaging films: It was evident that FeO-infused films have a high potential for absorbing oxygen, thus they have reduced OTR properties. The films infused with ZnO were observed to be potential antimicrobial films. Therefore, both the FeO and ZnO-infused films were combined to form a double-layer Nano-Biothermoplastic film. The mechanism of developing double-layer Nano-Biothermoplastic film is illustrated in the graphical abstract of this manuscript. The FeO-infused films formed the outer layer of Nano-Biothermoplastic film that may absorb oxygen molecules to reduce the OTR of the film. The inner layer (Food contact layer) consists of ZnO-infused films that may reduce the microbial growth rate in food products. The average thickness, tensile strength, elongation at break, OTR, WVTR and swelling index of the double layer nano-biothermoplastic film was estimated to be 0.95 ± 0.23 mm, 19.45 ± 2.54 MPa, 88.44 ± 5.32 %, 7.56 ± 0.23 cm3μmm-2d^{-1} kPa^{-1}, 0.52 ± 0.03 g $s^{-1}m^{-1}Pa^{-1}$, and 63.17 ± 0.58 %, respectively. Hypothesized Mechanism of Nano-biothermoplastic films: The diffusion of moisture from food samples facilitates the enlargement of micropores and release of nanoparticles from the biothermoplastic films. The food contact layer contains ZnO nanoparticles, that diffuse into the food products and follow its mechanism of action (as mentioned above in antimicrobial activity of nanoparticles) to reduce the growth of microbes in food. The outer FeO layer protects the oxidation of food, by absorbing atmospheric free oxygens and it also reduces the infestation possibility of atmospheric microbes into food products. Thus, the produced double-layer nano-biothermoplastic films can serve as potential food packaging system aid.

3.3. Diffusion kinetic of nanoparticles from Nano-Biothermoplastic films

The meat thickness was optimized with minimum inhibition of bacteria and diffusivity (D) of active compounds. The 0.5 cm thickness of the mutton meat was observed to possess reduced microbial growth on the side that was not in interaction with nanoparticles-infused bio-thermoplastic films. Consecutively, it was chosen as the optimized thickness for the storage of film-packed mutton meat. This improved effect of the antibacterial activity of nanoparticles could be due to their greater diffusivity in mutton meat. As 0.5 cm thick meat was selected from one side application of Nano-Biothermoplastic film, 1 cm thick meat was selected for applying the Nano-Biothermoplastic film package on all surfaces of the meat for diffusion kinetics analysis and shelf-life estimation. Chicken meat of 1 cm thickness was examined to have reduced microbial growth on the side that was not in interaction with nanoparticle-fused Biothermoplastic film. This optimized thickness of chicken meat was considerably ($P < 0.05$) higher than mutton meat samples. This may be attributed to the high moisture content in chicken meat facilitating effective nanoparticle diffusion into the chicken meat. The 1 cm thick meat was selected for one side of the Nano-Biothermoplastic film application, thus 2 cm thick meat was selected for applying edible film package on all sides of the meat for diffusion kinetic analysis and shelf life estimation.

Fig. 5, depicts the diffusion kinetics of ZnO and FeO nanoparticles into meat at different storage conditions. The equilibrium condition in nanoparticle diffusion from film to meat was not achieved; this could be due to the difference in the resistance provided by the meat sample and the film matrix. The resistance provided by the meat system is proficiently high than the film matrix (swelling in the film matrix also facilitates the drive of the nanoparticles in the film). Therefore, it might not be possible for achieving equilibrium among two solid matrices with different resistance (without the application of external force). The extreme release proficiency of ZnO and FeO into mutton meat for storage at 4 °C was observed to be having a considerable difference ($P < 0.05$) with samples stored at 10 °C. The maximum release efficiency of

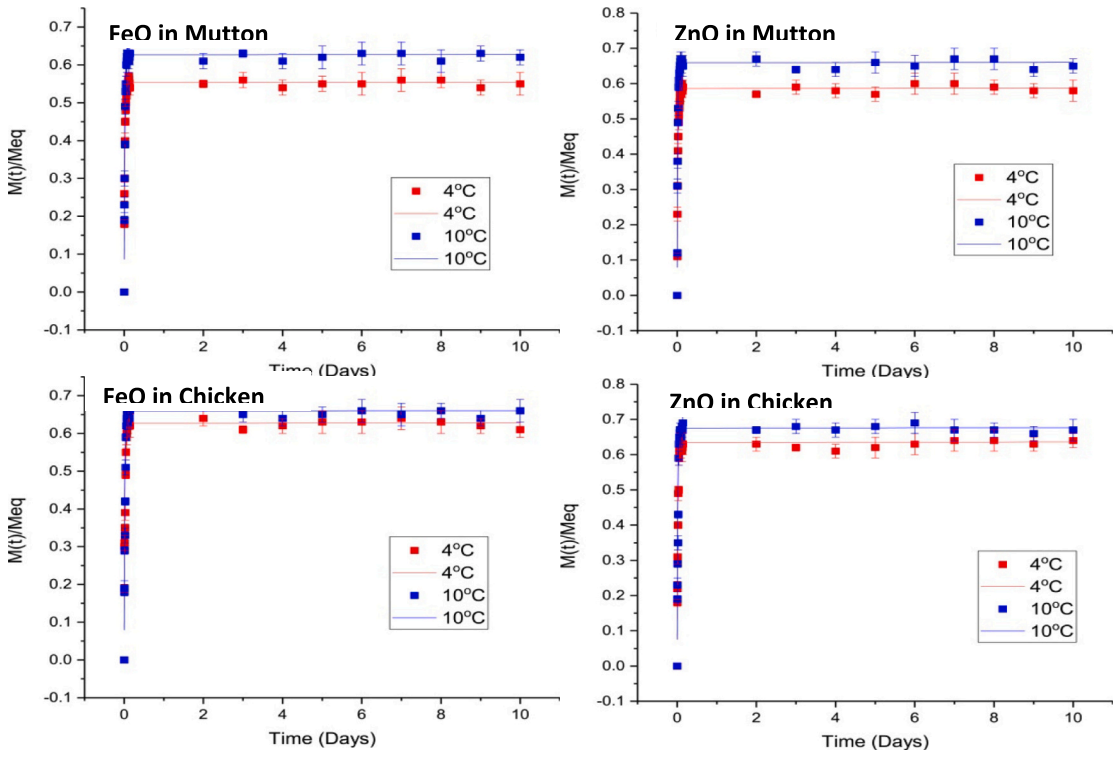

Fig. 5. Diffusion kinetics of nanoparticles into meat system.

Table 4
Diffusive kinetic parameter of nanomaterials into meat.

Diffusion through		Mutton meat (1 cm thickness)		Chicken meat (2 cm thickness)	
Temperature		4 °C	10 °C	4 °C	10 °C
τ (s)	ZnO	3873 ± 71	3219 ± 35	3149 ± 43	3009 ± 36
	FeO	3876 ± 62	3211 ± 32	3152 ± 41	3023 ± 32
D (cm^2/s)	ZnO	$0.72 \times 10^{-9} \pm 0.02 \times 10^{-9}$	$0.75 \times 10^{-9} \pm 0.02 \times 10^{-9}$	$0.76 \times 10^{-9} \pm 0.04 \times 10^{-9}$	$0.81 \times 10^{-9} \pm 0.03 \times 10^{-9}$
	FeO	$0.66 \times 10^{-9} \pm 0.04 \times 10^{-9}$	$0.71 \times 10^{-9} \pm 0.03 \times 10^{-9}$	$0.70 \times 10^{-9} \pm 0.03 \times 10^{-9}$	$0.77 \times 10^{-9} \pm 0.02 \times 10^{-9}$
F_X	ZnO	0.51 ± 0.03	0.42 ± 0.01	0.45 ± 0.03	0.40 ± 0.04
	FeO	0.55 ± 0.02	0.46 ± 0.04	0.46 ± 0.02	0.42 ± 0.02
R (s/cm)	ZnO	2.77×10^9	2.67×10^9	5.26×10^9	4.94×10^9
	FeO	3.03×10^9	2.82×10^9	5.71×10^9	5.19×10^9
R^2	ZnO	0.9963	0.9961	0.9875	0.9669
	FeO	0.9945	0.9889	0.9601	0.9627

Symbols: τ – Polymer relaxation time; D – Active compound diffusion coefficient; X_F – Deviation of the transport mechanism from the ideal Fickian behavior; R – Resistance of meat to active compound diffusion; R^2 – Model coefficient of determination.

ZnO and FeO in chicken meat, when stored at 4 and 10 °C, was found not to be significantly different ($P > 0.05$). This insignificant extreme release efficiency could be attributed to high moisture present in chicken meat than in mutton meat. The results also show that the greater storage temperature positively influences the dispersal of active compounds. This could result in the free-flowing of water molecules within the meat system at higher temperatures. But meat cannot be stored at higher temperature conditions because microbiota in meat could use these free water molecules for their rapid growth.

From the diffusion kinetics data, mathematical models (predictive) were developed by using a kinetic model equation (Eq. (2)). The solid line in the kinetic figure represents the greatest fit model curves of diffusion. The kinetic parameters calculated from the diffusivity model for nanoparticle diffusion into meat samples are given in Table 4. The diffusivity of ZnO and FeO nanoparticles into mutton meat was observed to be $0.72 \times 10^{-9} \pm 0.02 \times 10^{-9}$ and $0.66 \times 10^{-9} \pm 0.04 \times 10^{-9}$, respectively at 4 °C. The diffusivity of ZnO and FeO nanoparticles in chicken meat was observed to be $0.76 \times 10^{-9} \pm 0.04 \times 10^{-9}$ and $0.70 \times 10^{-9} \pm 0.03 \times 10^{-9}$, respectively at 4 °C. This significant ($P < 0.05$) increase in diffusivity of nanoparticles into chicken meat may be ascribed to the elevated moisture of the chicken meat than mutton meat. The diffusivity of nanoparticles was observed to be slightly increased at the elevated temperature of 10 °C. This could be because of the free movement of water and oil molecules inside the meat samples. The deviation of nanoparticle diffusion from fickian behavior and polymer relaxation time for diffusion of nanoparticles into chicken meat was observed to be considerably ($P < 0.05$) low, in comparison with mutton meat. This reduction in X_F and polymer relaxation time may also be attributed to the high moisture content of chicken meat that facilitates the free motion of nanoparticles in the meat system.

The moisture present in meat may diffuse to Biothermoplastic films. This moisture diffusion could result in the swelling of starch molecules, which in turn can facilitate the higher release of nanoparticles from the film into the meat. Consecutively, to understand the swelling influence of the film with the diffusion of nanoparticles, the swelling index of edible films was compared with nanoparticles diffusion into the meat. Fig. 6, illustrates the effect of the swelling index on the diffusive kinetics of nanoparticles in meat samples. In all the analysis samples, the

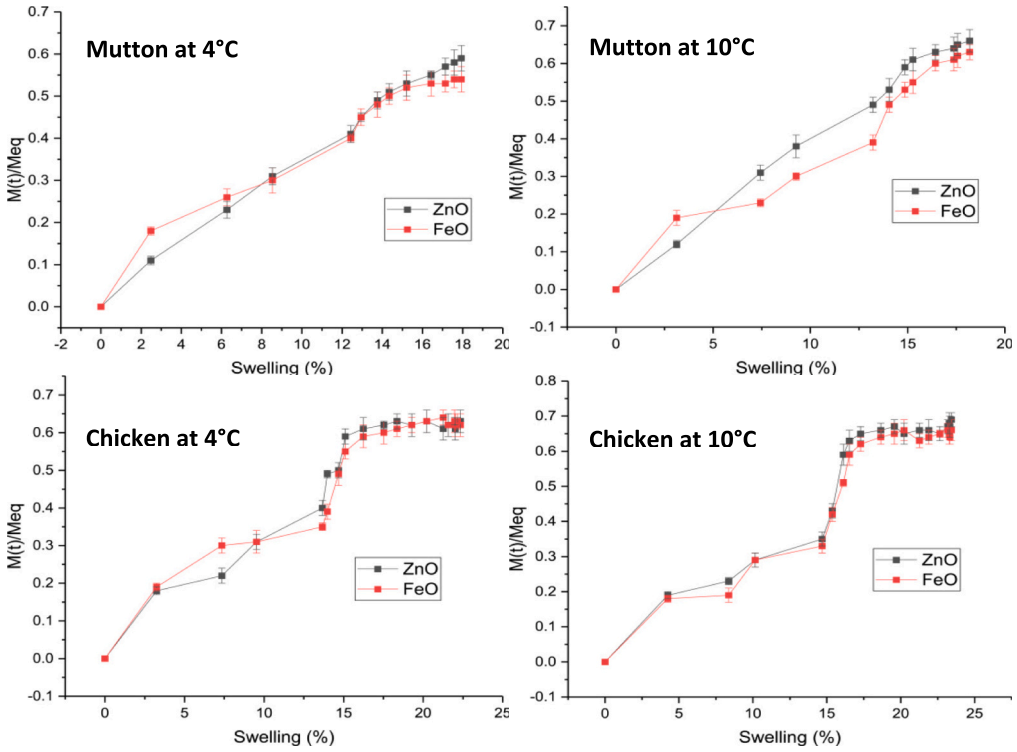

Fig. 6. Effect of the swelling index on the diffusion of nanoparticles into the meat system.

diffusion rate of nanoparticles was observed to be increasing with a rise in the swelling behavior of the bio-thermoplastic film. The maximum diffusion of nanoparticles in both chicken and mutton meat was observed to be achieved at a swelling percentage of 18 %. The swelling index of the starch-based films depends on the hydrogen bonding capability of the starch and okra mucilage polysaccharide (natural plasticizer). These molecules tend to hold a high amount of water molecules, which in turn results in the swelling of films. We have already studied and reported the effect on swelling of starch-based films with cross-linkers (e.g. Citric acid) and concentration of cellulose (e.g. sugarcane bagasse cellulose) [7,9]. Therefore, an increase in the concentration of cellulose and the addition of cross-linkers will help in reducing the swelling index of the starch-based films. The effect of storage temperature on the swelling percentage of bio-thermoplastic films was examined not to considerably ($P > 0.05$) affect the flow of nanoparticles inside the meat. This indicates that the rate of diffusion of nanoparticles is not entirely dependent on the temperature of storage. This phenomenon may be ascribed to the particle size of nanoparticles in comparison with other biological and synthetic active compounds. The meat products are prone to autolysis and microbial contamination at elevated temperatures. Therefore, the meat samples were only stored at 4 °C to study the effect of Nano-Biothermoplastic films on their shelf life.

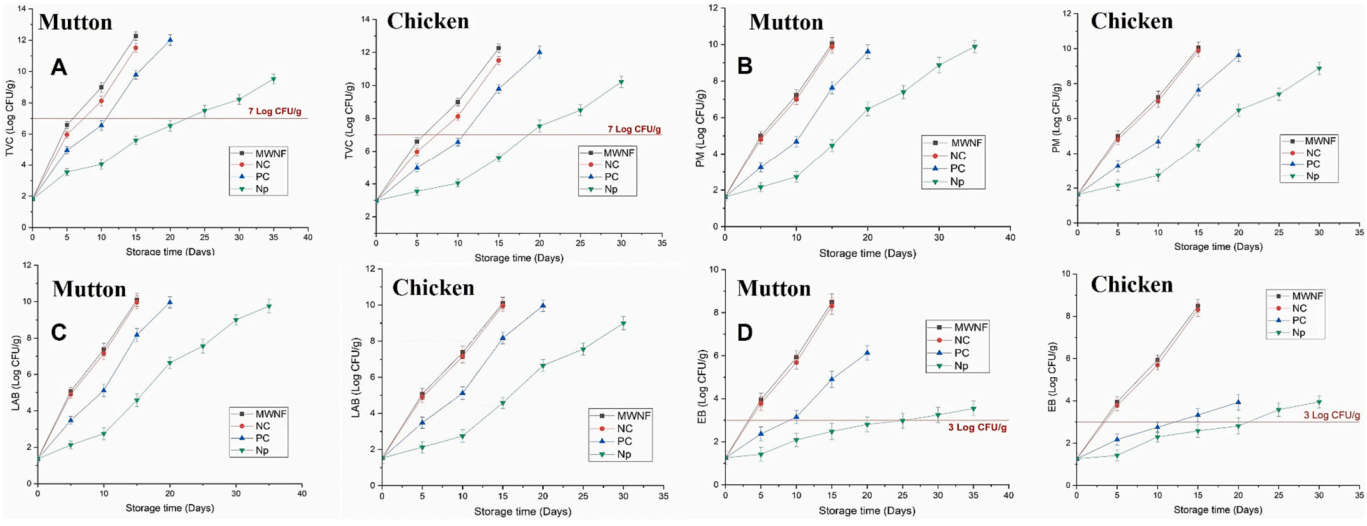

Fig. 7. Effect of double layer Nano-biothermoplastic packaging system in the total viable count, *Pseudomonads*, *Lactobacilli*, *Enterobacteriaceae* count of mutton and chicken meat system [Abbreviation: MWNF – Meat without Nano-biothermoplastic Film; NC – Negative Control (meat wrapped in biothermoplastic films without nanoparticles); PC - Positive Control (meat wrapped with biothermoplastic films containing commercial BHT); NP – Meat samples wrapped with Nano-biothermoplastic films].

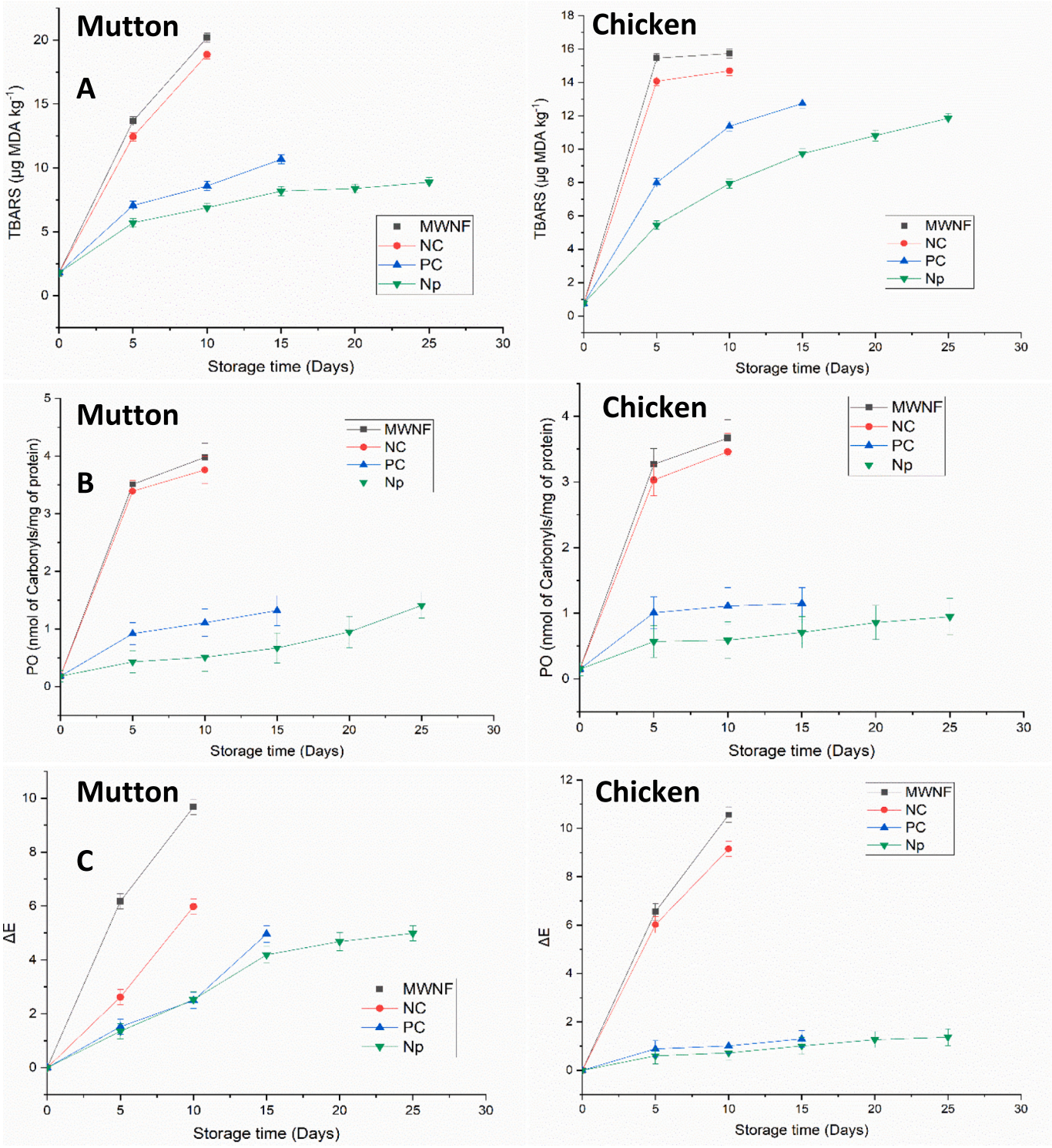

Fig. 8. Effect of Nano-Biothermoplastic packaging films on lipid oxidation, protein oxidation, color characteristics of chicken and mutton meat [Abbreviation: MWNF – Meat without Nano-biothermoplastic Film; NC – Negative Control (meat wrapped in biothermoplastic films without nanoparticles); PC - Positive Control (meat wrapped with biothermoplastic films containing commercial BHT); NP – Meat samples wrapped with Nano-biothermoplastic films].

3.4. Effect of Nano-Biothermoplastic films on the shelf-life of chicken and mutton meat

The microbial quality of food decides its shelf-life. According to FAO, the major factor for estimating the shelf life of food products is Total Viable Count (TVC) [28]. Fig. 7A depicts the effect of Nano-Biothermoplastic films on the TVC of mutton and chicken meat. The nanoparticle-infused test sample of both chicken and mutton meat showed a significant decrease ($P < 0.05$) in TVC in comparison with both positive and negative controls. The maximum acceptable level of TVC for the consumption of meat products was reported to be 7 Log CFU/g [28,44]. Therefore, the shelf life of chicken and mutton meat samples was observed to be extended up to 20 and 15 days, respectively by a double-layer Nano-Biothermoplastic packaging system. Many researchers have explained the importance of enumerating *Pseudomonads* counts in meat products that may play a significant part in meat microbiota [45]. The growth of *Pseudomonads* in food products facilitates the production of many lipolytic and proteolytic enzymes that may deteriorate the nutrient quality of food products to facilitate microbial growth. Fig. 7B illustrates the effect of Nano-Biothermoplastic films on the *Pseudomonads* count of chicken and mutton meat. The double-layer Nano-Biothermoplastic packaging system was examined to considerably ($P < 0.05$) affect the growth of *Pseudomonads* in chicken and mutton meat. The growth of *Lactobacilli* in meat samples has both useful and ill effects. The lactic acids produced by *Lactobacilli* can inhibit the growth of other microbes in meat [46,47]. The decrease in meat pH is due to the overproduction of lactic acid, which makes the meat incompatible for consumption. Fig. 7C shows the effect of Nano-Biothermoplastic films on the *Lactobacilli* count of chicken and mutton meat. The *Lactobacilli* count of chicken and mutton meat was also found to be significantly ($P < 0.05$) reduced by the double-layer Nano-Biothermoplastic packaging system.

The *Enterobacteriaceae* growth in meat products has been given as a pathogen-indicating factor by FAO [24,28,48]. The acceptable limit of *Enterobacteriaceae* count for the consumption of meat products was reported to be 3 Log CFU/g. Fig. 7D depicts the effect of Nano-Biothermoplastic films on the *Enterobacteriaceae* count of chicken and mutton meat. The double-layer Nano-Biothermoplastic packaging system showed a significant effect ($P < 0.05$) against the growth of *Enterobacteriaceae* in chicken and mutton meat. The test sample of both the mutton and chicken meat was observed to be within the acceptable limit for the estimated shelf life of 20 and 15 days (for storage at 4 °C), respectively.

The growth of putrefying microbes greatly causes the chemical deterioration of meat products. Various enzymes are produced by *Pseudomonads*, these enzymes cause the release of fatty acids from the meat fat. These free fatty acids undergo oxidation, affecting the chemical properties of meat products. The off-flavors or rancidity of meat was reported to be caused by oxidative by-products of fatty acids.

Fig. 8A illustrates the effect of Nano-Biothermoplastic films on the thiobarbituric acid reactive substance (TBARS) values of mutton and chicken meat stored at 4 °C. The double-layer Nano-Biothermoplastic packaging system showed a significant effect ($P < 0.05$) against the TBARS estimates of chicken and mutton meat. Greene & Cumuze [49], noted that 0.6–2.0 mg MDA/kg of meat is required to detect off-flavors even by an inexperienced consumer panel. Tarladgis et al. [50] reported that the MDA level of 0.5–1 mg MDA/kg of meat is necessary for off-flavor detection by an experienced consumer panel. The levels of MDA in both the chicken and mutton meat samples were observed to be well within the limit for off-flavor detection. Fig. 8B illustrates the effect of Nano-Biothermoplastic films on the Protein Oxidation (PO) of mutton and chicken meat stored at 4 °C. The double-layer Nano-Biothermoplastic packaging system showed a significant ($P < 0.05$) effect in the PO values of both mutton and chicken meat. This effective reduction of protein and lipid oxidation in both mutton and chicken meat may be ascribed to the high oxygen-scavenging capacity of FeO and ZnO nanoparticles. The color evaluation of meat samples during storage is important for consumer acceptance [51]. Fig. 8C depicts the effect of Nano-Biothermoplastic films on the color characteristics of mutton and chicken meat stored at 4 °C. Considerable differences ($P < 0.05$) in ΔE values were observed among test and control samples of both mutton and chicken meat. These results indicate the active ingredient effect of nanoparticles on color retention of mutton meat. Thus, the analysis of lipid oxidation, protein oxidation, and color characteristics proved the effectiveness of the double-layer Nano-Biothermoplastic packaging system in the control of chemical and physical deterioration in both mutton and chicken meat.

4. Conclusions

The clove extract was observed to hold good potential for the synthesis of stable nanoparticles with a high nano conversion rate. The synthesized FeO and ZnO nanoparticles were examined to have high antioxidant and antimicrobial properties. Consecutively, they were selected as potential active ingredients for the production of nanoparticle-infused bioactive thermoplastic packaging films. The biothermoplastic films infused with FeO nanoparticles showed high oxygen scavenging activity with a low oxygen transfer level. The biothermoplastic films infused with ZnO nanoparticles showed high antimicrobial activity. Consecutively, both films were combined to form a double-layer Nano-Biothermoplastic packaging system for food preservation. The distribution of nanoparticles in starch-based biothermoplastic films was examined to be influenced by the amorphous property of starch molecules. The diffusion of nanoparticles in starch base biothermoplastic films was studied to be influenced by the swelling index of the film. The amorphous property of starch molecules was also studied to be masking the crystalline characteristics of nanoparticles in Nano-Biothermoplastic films. The diffusion of nanoparticles from the Nano-Biothermoplastic packaging system was found to influence the microbial, chemical, and color characteristics of mutton and chicken meat stored at 4 °C. Consecutively, the infusion of nanoparticles to develop bioactive starch-based thermoplastic films was observed to be a potential packaging system for the shelf-life extension of food products.

CRediT authorship contribution statement

Chandra Mohan Chandrasekar: Conceptualization, Methodology, Investigation, Supervision, funding acquisition, Project administration and writing original draft.

Luca Nespoli: Investigation, Data Curation and Formal analysis.

Tommaso Bellesia: Investigation, Data Curation and Formal analysis.

Masoud Ghaani: Validation and Data Curation.

Stefano Farris: Supervision and Review/editing.

Diego Romano: Supervision, Resources and Review/editing.

Declaration of competing interest

The authors declare that they have no known competing financial interests or personal relationships that could have appeared to influence the work reported in this paper.

The authors declare that there are no conflicts of interest.

Acknowledgement

The first author would like to express his sincere thanks to the Council of Scientific and Industrial Research – CSIR for the award of a senior research fellowship (No.: 09/468/0500/2016/EMR-I).

Appendix A. Supplementary data

Supplementary data to this article can be found online at https://doi.org/10.1016/j.ijbiomac.2023.127689.

References

[1] C. Chandra Mohan, K.R. Rakhavan, K. Sudharsan, K. Radha Krishnan, S. Babuskin, M. Sukumar, Design and characterization of spice fused tamarind starch edible packaging films, LWT Food Sci. Technol. 68 (2016) 642–652, https://doi.org/10.1016/j.lwt.2016.01.004.

[2] C. Chandra Mohan, K. Harini, B. Vajiha Aafrin, U. Lalitha Priya, P. Maria Jenita, S. Babuskin, S. Karthikeyan, K. Sudarshan, V. Renuka, M. Sukumar, Extraction and characterization of polysaccharides from tamarind seeds, rice mill residue, okra waste and sugarcane bagasse for its bio-thermoplastic properties, Carbohydr. Polym. 186 (2018) 394–401, https://doi.org/10.1016/j.carbpol.2018.01.057.

[3] R. Colussi, V.Z. Pinto, S.L. Mello El Halal, E.D. Rosa Zavareze, A.R. Guerra Dias, Physical, mechanical, and thermal properties of biodegradables films of rice starch, Curr. Agric. Sci. Technol. 20 (n.d.) 1–9.

[4] M. Majzoobi, Y. Pesaran, G. Mesbahi, M.T. Golmakani, A. Farahnaky, Physical properties of biodegradable films from heat-moisture-treated rice flour and rice starch, Starch/Staerke (2015), https://doi.org/10.1002/star.201500102.

[5] R. Colussi, V.Z. Pinto, S.L.M. El Halal, B. Biduski, L. Prietto, D.D. Castilhos, E. da R. Zavareze, A.R.G. Dias, Acetylated rice starches films with different levels of amylose: mechanical, water vapor barrier, thermal, and biodegradability properties, Food Chem. (2017), https://doi.org/10.1016/j.foodchem.2016.10.129.

[6] T.J. Gutiérrez, V.A. Alvarez, Cellulosic materials as natural fillers in starch-containing matrix-based films: a review, Polym. Bull. (2017), https://doi.org/10.1007/s00289-016-1814-0.

[7] C. Chandra Mohan, K. Harini, S. Karthikeyan, K. Sudharsan, M. Sukumar, Effect of film constituents and different processing conditions on the properties of starch based thermoplastic films, Int. J. Biol. Macromol. (2018), https://doi.org/10.1016/j.ijbiomac.2018.09.161.

[8] V.G.L. Souza, J.R.A. Pires, É.T. Vieira, I.M. Coelhoso, M.P. Duarte, A.L. Fernando, Shelf life assessment of fresh poultry meat packaged in novel bionanocomposite of chitosan/montmorillonite incorporated with ginger essential oil, Coatings 8 (2018) 1–17, https://doi.org/10.3390/coatings8050177.

[9] K. Harini, C. Chandra Mohan, K. Ramya, S. Karthikeyan, M. Sukumar, Effect of *Punica granatum* peel extracts on antimicrobial properties in Walnut shell cellulose reinforced bio-thermoplastic starch films from cashew nut shells, Carbohydr. Polym. 184 (2018) 231–242, https://doi.org/10.1016/j.carbpol.2017.12.072.

[10] C. Medina-Jaramillo, O. Ochoa-Yepes, C. Bernal, L. Famá, Active and smart biodegradable packaging based on starch and natural extracts, Carbohydr. Polym. 176 (2017) 187–194, https://doi.org/10.1016/j.carbpol.2017.08.079.

[11] S. Ni, H. Zhang, P.M. Godwin, H. Dai, H. Xiao, ZnO nanoparticles enhanced hydrophobicity for starch film and paper, Mater. Lett. 230 (2018) 207–210, https://doi.org/10.1016/j.matlet.2018.07.075.

[12] Z. Foltynowicz, A. Bardenshtein, S. Sängerlaub, H. Antvorskov, W. Kozak, Nanoscale, zero valent iron particles for application as oxygen scavenger in food packaging, Food Packag. Shelf Life 11 (2017) 74–83, https://doi.org/10.1016/j.fpsl.2017.01.003.

[13] M.N. Lakhan, R. Chen, A.H. Shar, K. Chand, A.H. Shah, M. Ahmed, I. Ali, R. Ahmed, J. Liu, K. Takahashi, J. Wang, Eco-friendly green synthesis of clove buds extract functionalized silver nanoparticles and evaluation of antibacterial and antidiatom activity, J. Microbiol. Methods 173 (2020), https://doi.org/10.1016/j.mimet.2020.105934.

[14] A. Babaei-Ghazvini, I. Shahabi-Ghahfarrokhi, V. Goudarzi, Preparation of UV-protective starch/kefiran/ZnO nanocomposite as a packaging film: characterization, Food Packag. Shelf Life 16 (2018) 103–111, https://doi.org/10.1016/j.fpsl.2018.01.008.

[15] M.S. Ghamsari, S. Alamdari, D. Razzaghi, M. Arshadi Pirlar, ZnO nanocrystals with narrow-band blue emission, JOL 205 (2019) 508–518, https://doi.org/10.1016/j.jlumin.2018.09.064.

[16] K. Sudharsan, C. Chandra Mohan, P. Azhagu Saravana Babu, G. Archana, K. Sabina, M. Sivarajan, M. Sukumar, Production and characterization of cellulose reinforced starch (CRT) films, Int. J. Biol. Macromol. 83 (2016) 385–395, https://doi.org/10.1016/j.ijbiomac.2015.11.037.

[17] T.P.R. dos Santos, M. Leonel, É.L. Garcia, E.L. do Carmo, C.M.L. Franco, Crystallinity, thermal and pasting properties of starches from different potato cultivars grown in Brazil, Int. J. Biol. Macromol. (2016), https://doi.org/10.1016/j.ijbiomac.2015.10.091.

[18] S. Ibrahim, H. El Saied, M. Hasanin, Active paper packaging material based on antimicrobial conjugated nano-polymer/amino acid as edible coating, J. King Saud Univ. Sci. 31 (2019) 1095–1102, https://doi.org/10.1016/j.jksus.2018.10.007.

[19] K. Harini, K. Ramya, M. Sukumar, Extraction of nano cellulose fibers from the banana peel and bract for production of acetyl and lauroyl cellulose, Carbohydr. Polym. (2018), https://doi.org/10.1016/j.carbpol.2018.08.081.

[20] M. Ghasemlou, N. Aliheidari, R. Fahmi, S. Shojaee-Aliabadi, B. Keshavarz, M. J. Cran, R. Khaksar, Physical, mechanical and barrier properties of corn starch films incorporated with plant essential oils, Carbohydr. Polym. 98 (2013) 1117–1126, https://doi.org/10.1016/j.carbpol.2013.07.026.

[21] K. Sudharsan, C. Chandra Mohan, Azhagu Saravana Babu, G. Archana, K. Sabina, M. Sivarajan, M. Sukumar, Production and characterization of cellulose reinforced starch (CRT) films, Int. J. Biol. Macromol. 83 (2016) 385–395, https://doi.org/10.1016/j.ijbiomac.2015.11.037.

[22] P. Fajardo, J.T. Martins, C. Fuciños, L. Pastrana, J.A. Teixeira, A.A. Vicente, Evaluation of a chitosan-based edible film as carrier of natamycin to improve the storability of Saloio cheese, J. Food Eng. 101 (2010) 349–356, https://doi.org/10.1016/j.jfoodeng.2010.06.029.

[23] C.C. Mohan, K. Harini, K. Sudharsan, K.R. Krishnan, M. Sukumar, Quorum quenching effect and kinetics of active compound from *S. aromaticum* and *C. cassia* fused packaging films in shelf life of chicken meat, LWT (2019), https://doi.org/10.1016/j.lwt.2019.01.061.

[24] C. Chandra Mohan, K. Radha Krishnan, S. Babuskin, K. Sudharsan, V. Aafrin, U. Lalitha Priya, P. Mariyajenita, K. Harini, D. Madhushalini, M. Sukumar, Active compound diffusivity of particle size reduced *S. aromaticum* and *C. cassia* fused starch edible films and the shelf life of mutton (*Capra aegagrus* hircus) meat, Meat Sci. 128 (2017) 47–59, https://doi.org/10.1016/j.meatsci.2017.02.001.

[25] J. Crank, The Mathematics of Diffusion. 2nd edn., (n.d.).

[26] S. Tautkus, L. Steponeniene, R. Kazlauskas, Determination of iron in natural and mineral waters by flame atomic absorption spectrometry, J. Serb. Chem. Soc. 69 (2004) 393–402, https://doi.org/10.2298/JSC0405393T.

[27] S. Ata, F.H. Wattoo, M. Ahmed, M.H.S. Wattoo, S.A. Tirmizi, A. Wadood, A method optimization study for atomic absorption spectrophotometric determination of total zinc in insulin using direct aspiration technique, Alexandria J. Med. 51 (2015) 19–23, https://doi.org/10.1016/j.ajme.2014.03.004.

[28] G. Heinz, P. Hautzinger, Meat Processing Technology for Small- to Medium-scale Producers, 2007.

[29] L. Barbosa-Pereira, G.P. Aurrekoetxea, I. Angulo, P. Paseiro-Losada, J.M. Cruz, Development of new active packaging films coated with natural phenolic compounds to improve the oxidative stability of beef, Meat Sci. 97 (2014) 249–254, https://doi.org/10.1016/j.meatsci.2014.02.006.

[30] S. Jafarzadeh, F. Ariffin, S. Mahmud, A.K. Alias, S.F. Hosseini, M. Ahmad, Improving the physical and protective functions of semolina films by embedding a blend nanofillers (ZnO-nr and nano-kaolin), Food Packag. Shelf Life 12 (2017) 66–75, https://doi.org/10.1016/j.fpsl.2017.03.001.

[31] A. Naveed Ul Haq, A. Nadhman, I. Ullah, G. Mustafa, M. Yasinzai, I. Khan, Synthesis approaches of zinc oxide nanoparticles: the dilemma of ecotoxicity, J. Nanomater. 2017 (2017), https://doi.org/10.1155/2017/8510342.

[32] A. Kumar, C.K. Dixit, Methods for characterization of nanoparticles, in: Advances in Nanomedicine for the Delivery of Therapeutic Nucleic Acids, 2017, https://doi.org/10.1016/B978-0-08-100557-6.00003-1.

[33] T.L. Doane, C.-H. Chuang, R.J. Hill, C. Burda, Nanoparticle ζ-Potentials, Acc. Chem. Res. 45 (2012) 317–326, https://doi.org/10.1021/ar200113c.

[34] A. Naskar, H. Khan, R. Sarkar, S. Kumar, D. Halder, S. Jana, Anti-biofilm activity and food packaging application of room temperature solution process based polyethylene glycol capped Ag-ZnO-graphene nanocomposite, Mater. Sci. Eng. C 91 (2018) 743–753, https://doi.org/10.1016/j.msec.2018.06.009.

[35] S.W. Hwang, A. Umar, G.N. Dar, S.H. Kim, R.I. Badran, Synthesis and characterization of iron oxide nanoparticles for phenyl hydrazine sensor applications, Sens. Lett. 12 (2014) 97–101, https://doi.org/10.1166/sl.2014.3224.

[36] A.T. Khalil, M. Ovais, I. Ullah, M. Ali, Z. Khan Shinwari, M. Maaza, Biosynthesis of iron oxide (Fe_2O_3) nanoparticles via aqueous extracts of *Sageretia thea* (Osbeck.) and their pharmacognostic properties, Green Chem. Lett. Rev. 10 (2017) 186–201, https://doi.org/10.1080/17518253.2017.1339831.

[37] H. Viltres, O.F. Odio, R. Borja, Y. Aguilera, E. Reguera, Magentite nanoparticle for arsenic remotion, J. Phys. Conf. Ser. (2017), https://doi.org/10.1088/1742-6596/792/1/012078.

[38] H. Esmailzadeh, P. Sangpour, F. Shahraz, J. Hejazi, R. Khaksar, Effect of nanocomposite packaging containing ZnO on growth of *Bacillus subtilis* and *Enterobacter aerogenes*, Mater. Sci. Eng. C 58 (2016) 1058–1063, https://doi.org/10.1016/j.msec.2015.09.078.

[39] J.L. Castro-Mayorga, M.J. Fabra, A.M. Pourrahimi, R.T. Olsson, J.M. Lagaron, The impact of zinc oxide particle morphology as an antimicrobial and when incorporated in poly(3-hydroxybutyrate-co-3-hydroxyvalerate) films for food packaging and food contact surfaces applications, Food Bioprod. Process. 101 (2017) 32–44, https://doi.org/10.1016/j.fbp.2016.10.007.

[40] N. Talebian, S.M. Amininezhad, M. Doudi, Controllable synthesis of ZnO nanoparticles and their morphology-dependent antibacterial and optical properties, J. Photochem. Photobiol. B Biol. (2013), https://doi.org/10.1016/j.jphotobiol.2013.01.004.

[41] R. Krishnamoorthy, J. Athinarayanan, V.S. Periyasamy, M.A. Alshuniaber, G. Alshammari, M.J. Hakeem, M.A. Ahmed, A.A. Alshatwi, Antibacterial mechanisms of zinc oxide nanoparticle against bacterial food pathogens resistant to beta-lactam antibiotics, Molecules 27 (2022), https://doi.org/10.3390/molecules27082489.

[42] M. Arakha, S. Pal, D. Samantarrai, T.K. Panigrahi, B.C. Mallick, K. Pramanik, B. Mallick, S. Jha, Antimicrobial activity of iron oxide nanoparticle upon modulation of nanoparticle-bacteria interface, Sci. Rep. 5 (2015), https://doi.org/10.1038/srep14813.

[43] F.M. Abdulsada, N.N. Hussein, G.M. Sulaiman, A. Al Ali, M. Alhujaily, Evaluation of the antibacterial properties of iron oxide, polyethylene glycol, and gentamicin conjugated nanoparticles against some multidrug-resistant bacteria, J. Funct. Biomater. 13 (2022), https://doi.org/10.3390/jfb13030138.

[44] C. Chandra Mohan, K.R. Rakhavan, K. Radha Krishnan, S. Babuskin, K. Sudharsan, P. Azhagu Saravana Babu, M. Sukumar, Development of predictive preservative model for shelf life parameters of beef using response surface methodology, LWT Food Sci. Technol. 72 (2016) 239–250, https://doi.org/10.1016/j.lwt.2016.04.019.

[45] D.A. G., J.M. Jay, M.J. Loessner, Modern Food Microbiology, 7th edn, Springer, New York, 2005.

[46] S. Petrou, M. Tsiraki, V. Giatrakou, I.N. Savvaidis, Chitosan dipping or oregano oil treatments, singly or combined on modified atmosphere packaged chicken breast meat, Int. J. Food Microbiol. (2012), https://doi.org/10.1016/j.ijfoodmicro.2012.04.002.

[47] S. Limbo, L. Torri, N. Sinelli, L. Franzetti, E. Casiraghi, Evaluation and predictive modeling of shelf life of minced beef stored in high-oxygen modified atmosphere packaging at different temperatures, Meat Sci. (2010), https://doi.org/10.1016/j.meatsci.2009.08.035.

[48] C.S. Chandra Mohan, R. Rakhavan Kavindapadi, K. Radha Krishnan, S. Babuskin, K. Sudharsan, P. Azhagu Saravana Babu, M. Sukumar, Impact of *S. aromaticum* and *C. cassia* incorporated edible films on shelf life of seer fish (*Scomberomorus guttatus*) stored at different temperature conditions, J. Food Process. Preserv. 41 (2017) 1–11, https://doi.org/10.1111/jfpp.13096.

[49] B.E. Greene, T.H. Cumuze, Relationship between TBA numbers and inexperienced panelists'assessments of oxidized flavor in cooked beef, J. Food Sci. (1982), https://doi.org/10.1111/j.1365-2621.1982.tb11025.x.

[50] B.G. Tarladgis, B.M. Watts, M.T. Younathan, L. Dugan, A distillation method for the quantitative determination of malonaldehyde in rancid foods, J. Am. Oil Chem. Soc. (1960), https://doi.org/10.1007/BF02630824.

[51] R. Bórnez, M.B. Linares, H. Vergara, Effect of different gas stunning methods on Manchega suckling lamb meat packed under different modified atmospheres, Meat Sci. (2010), https://doi.org/10.1016/j.meatsci.2009.11.008.